

Award Number:
W81XWH-10-1-0506

TITLE:
Imaging Molecular Signatures of Breast Cancer with X-ray-Activated
Nanophosphors

PRINCIPAL INVESTIGATOR:
Colin M. Carpenter

CONTRACTING ORGANIZATION:
The Leland Stanford Junior University
Stanford CA 94305

REPORT DATE:
September 2012

TYPE OF REPORT:
Annual U|↑↑áã]

PREPARED FOR: U.S. Army Medical Research and Materiel Command
Fort Detrick, Maryland 21702-5012

DISTRIBUTION STATEMENT:

Approved for public release; distribution unlimited

The views, opinions and/or findings contained in this report are those of the author(s) and should not be construed as an official Department of the Army position, policy or decision unless so designated by other documentation.

REPORT DOCUMENTATION PAGE

Form Approved
OMB No. 0704-0188

Public reporting burden for this collection of information is estimated to average 1 hour per response, including the time for reviewing instructions, searching existing data sources, gathering and maintaining the data needed, and completing and reviewing this collection of information. Send comments regarding this burden estimate or any other aspect of this collection of information, including suggestions for reducing this burden to Department of Defense, Washington Headquarters Services, Directorate for Information Operations and Reports (0704-0188), 1215 Jefferson Davis Highway, Suite 1204, Arlington, VA 22202-4302. Respondents should be aware that notwithstanding any other provision of law, no person shall be subject to any penalty for failing to comply with a collection of information if it does not display a currently valid OMB control number. **PLEASE DO NOT RETURN YOUR FORM TO THE ABOVE ADDRESS.**

1. REPORT DATE (DD-MM-YYYY)

1 September 2012

2. REPORT TYPE

ANNUAL SUMMARY

3. DATES COVERED (From - To)

1 Sep 2011 – 31 Aug 2012

4. TITLE AND SUBTITLE

Imaging Molecular Signatures of Breast Cancer with X-ray-Activated Nanophosphors

5a. CONTRACT NUMBER

5b. GRANT NUMBER
W81XWH-10-1-0506

5c. PROGRAM ELEMENT NUMBER**6. AUTHOR(S)**

COLIN CARPENTER

colincarpenter@stanford.edu

5d. PROJECT NUMBER**5e. TASK NUMBER****5f. WORK UNIT NUMBER****7. PERFORMING ORGANIZATION NAME(S) AND ADDRESS(ES)**

The Leland Stanford Junior University
Utanford CA 94305

8. PERFORMING ORGANIZATION REPORT NUMBER**9. SPONSORING / MONITORING AGENCY NAME(S) AND ADDRESS(ES)**

U.S. ARMY MEDICAL RESEARCH
AND MATERIAL COMMAND
FORT DETRICK, MARYLAND
21702-5012

10. SPONSOR/MONITOR'S ACRONYM(S)**11. SPONSOR/MONITOR'S REPORT NUMBER(S)****12. DISTRIBUTION / AVAILABILITY STATEMENT**

APPROVED FOR PUBLIC RELEASE; DISTRIBUTION UNLIMITED

13. SUPPLEMENTARY NOTES**14. ABSTRACT**

The first year of this research program developed the foundation for Radioluminescence Imaging (RLI) and Radioluminescence Tomography (RLT). The second year of this research program, detailed in this report, was dedicated to optimizing the instrumentation for the RLT imager, developing a technique to image multiple phosphor targets simultaneously, and creating the instrumentation for percutaneous imaging of RLI. Overall, sensitivity has been improved to a level on par with fluorescent imaging. The inclusion of a filter wheel to spectrally select the phosphor photon emission has enabled multiplexed imaging, which was shown to linearly quantify multiple molecular contrasts simultaneously, saving time and resources; this system was demonstrated in small animal phantoms. The percutaneous RLI system was developed to enable imaging of targeted nanophosphors through a biopsy needle. This system is able to fit in a standard 10 gauge biopsy needle. We have thus completed aims 1, 2, and 3 of the grant. We are beginning aim 4: pre-clinical testing in a small animal breast tumor model. This preclinical testing will be performed in our RLT imager.

For this second round of funding, we have an additional 1 peer-reviewed journal publications, and 4 more conference abstracts for this project as a direct result of this funding. The cumulative total results of this grant is: 7 journal publications, including 3 first author; 12 conference abstracts, and 4 courses taken. Several postdoctoral fellows are now being mentored and working in RLI.

15. SUBJECT TERMS

BREAST CANCER, IMAGING, MOLECULAR IMAGING, X-RAY, NANOPARTICLES

16. SECURITY CLASSIFICATION OF:

a. REPORT
U

b. ABSTRACT
U

c. THIS PAGE
U

17. LIMITATION OF ABSTRACT

UU

18. NUMBER OF PAGES

18

19a. NAME OF RESPONSIBLE PERSON

19b. TELEPHONE NUMBER (include area code)

Table of Contents

	<u>Page</u>
Introduction.....	4
Body.....	4
Key Research Accomplishments.....	9
Reportable Outcomes.....	9
Conclusion.....	10
References.....	10
Appendices.....	11

INTRODUCTION

Improved molecular imaging tools are needed to further research and development, and enable translation into the clinic to improve disease diagnosis and treatment. Radioluminescence Imaging (RLI) / Tomography (RLT) have been developed in this grant to accomplish these goals. RLI utilizes biologically compatible phosphor nanoparticles to produce images of molecular contrasts, which provide expansive disease-specific information. This is particularly relevant for breast cancer because of the limited specificity of current breast cancer imaging tools. Additionally, there is a lack of interventional tools to help perform image-guided biopsies and surgeries. Towards these goals, year 2 of this fellowship meant to further optimize the RLI instrumentation for sensitivity, to develop an RLI biopsy tool, and to demonstrate the multiplexing ability of this modality, which is a significant advantage of this modality compared to current molecular imaging tools.

For this second year of funding, we have an additional 1 peer-reviewed journal publications, and 4 more conference abstracts for this project as a direct result of this funding. As of today, the total results of this grant are: 7 journal publications, including 3 first author; 12 conference abstracts, and 4 courses taken. Several postdoctoral fellows are now being mentored and working in RLI.

For the second-year training goals, this grant has provided for extensive study in molecular targeting of cancer, and the opportunity to mentor 2 postdoctoral fellows in RLI and molecular imaging. Aims 1 & 2 & 3 of the grant are completed. Aim 4, pre-clinical testing in a small animal breast tumor model, is currently in preparation. ACURO approval for the animal protocol required for aim 4 is currently under review with the DOD (IACUC approval at Stanford is already granted).

BODY

Research Accomplishments: SOW Aim 2: Imaging Hardware Development: Increased Sensitivity

Meeting the goals outlined in aim 2, we improved the sensitivity of Radioluminescent Imaging by incorporating leaded glass in front of the camera, a chiller, and a filter wheel. The 3/8" thick glass sheet was custom machined (Ray-bar, Inc) to attach to our RLI imager, and attenuates the X-rays by >99.999% before they hit the CCD and cause increased noise in the pixels. Due to this improvement, we have seen a dramatic decrease in the stochastic X-ray noise in the CCD; this has enabled integration times of over 20 seconds. The liquid chiller for the CCD camera brings the CCD temperature down to -85C.

We demonstrated the improvements to the RLI system by imaging an organic phosphor (PDOT) and water (H₂O) with the old setup and the new setup. We placed the samples in our imaging box and irradiated them with 50 and 80 kVp x-rays using a superficial X-ray irradiator. For the old samples, we shut off the chiller and removed the X-ray glass. Using ideal gain and integration settings, signal for the PDOTs and H₂O were nearly indistinguishable from the noise of about 200 counts, due to the high X-ray noise from the incident irradiation, and the dark counts from thermal noise on the CCD. After connecting the chiller and installing the leaded glass in front of the CCD lens, we then repeated the experiment with ideal settings. As shown in Figure 1, signal for the phosphor was increased by a factor of 8 over the old setup.

These improvements have increased our sensitivity to below 10 μ g/ml. This sensitivity should be sufficient to image receptor binding (e.g. VEGF or HER-2) at concentrations of ~15 nM, which is sufficient for molecular imaging.

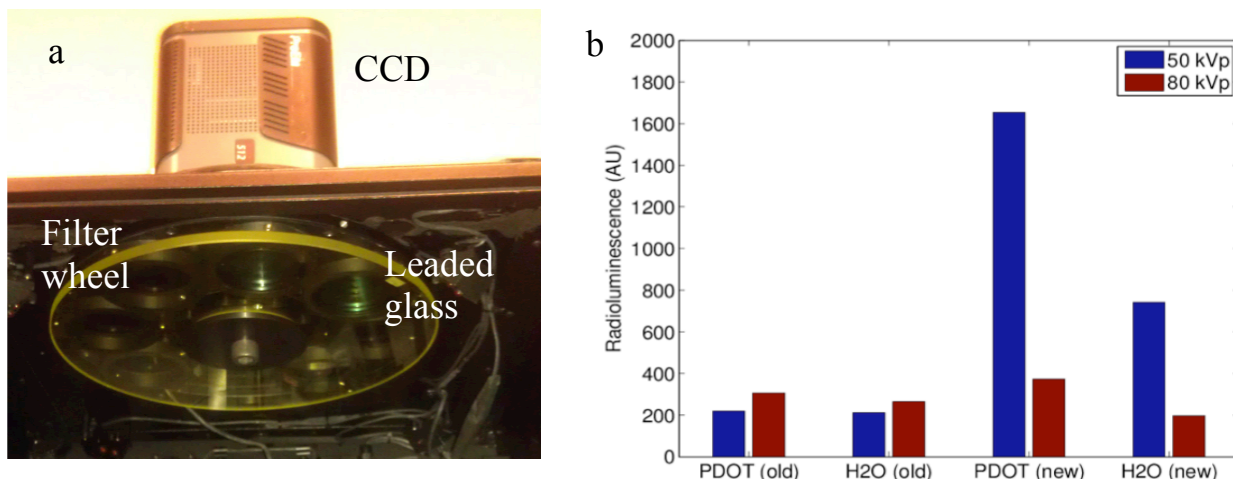


Figure 1: RLT system with improved sensitivity. (a) 3/8” thick leaded glass prevents X-ray noise from hitting the CCD, and enables longer integration times. The filter wheel enables spectral selectivity. (b) Intensity emitted from phosphors (PDOT) and water. The increase in intensity of the (new) vs (old) samples demonstrates the longer integration times possible.

Research Accomplishments: SOW Aim 2: Imaging Hardware/Software Development: Multiplexing

The ability to image multiple nanoparticle-based contrast agents simultaneously is a key advantage of RLI over other molecular imaging modalities, such as PET, and many types of fluorescence imaging. Since the radioluminescent nanoparticles emit optical light at unique wavelengths, depending on their lanthanide dopant, we are able to selectively image the unique phosphors with the use of optical filters. We demonstrated this technique by separating two distinct nanophosphor contrast agents in gelatin phantoms and a small animal phantom.

To enable multiplexed imaging, both hardware and software were developed. A filter wheel (Caliper Life Sciences, Alameda, CA) was mounted on our imager with 2 filters for 2 different phosphor nanoparticles (548nm: CaF₂:Tb, 700nm: CaF₂:Eu). Leaded glass was placed above the subject. To form images of the concentrations, c , of each of these particles, the light emitted, ϕ , was recorded over the several optical spectral regions defined by filter f_1 and filter f_2 to form images of the subject, $i_1 = \phi(f_1)$ and $i_2 = \phi(f_2)$. These images, and the pre-recorded reference spectra, ϵ , for Ba_{0.55}Y_{0.3}F₂:Tb³⁺, (ϵ_{Tb}), Ba_{0.55}Y_{0.3}F₂:Eu³⁺, (ϵ_{Eu}), were input into a linear-least squares algorithm to extract the contributions from each nanophosphor. Reference spectra were collected with a calibrated spectrometer, thus enabling a quantitative comparison between the nanophosphors.

To validate the ability of this method to image multiple nanophosphors simultaneously, five phantoms (99% DI water, 1% agarose) were fabricated containing Tb³⁺ and Eu³⁺ doped RLNPs of linearly varying concentrations (in units of mg/ml) and mixed in the following ratios: (0:10; 2.5:7.5; 5:5; 7.5:2.5; and 10:0). Figure 2(a) displays the unmixed images for linearly increasing (top-to-bottom) amounts of Tb³⁺-doped RLNPs on the left, and decreasing (top-to-bottom) Eu³⁺-doped RLNPs on the right, at each concentration. The median values for each region of interest were plotted with respect to concentration. Figure 2(b) shows the median raw signal detected from each nanophosphor concentration. Figure 2(c) demonstrates this method’s efficacy in separating the nanophosphors; the correlation between the samples was ($r = -0.98$).

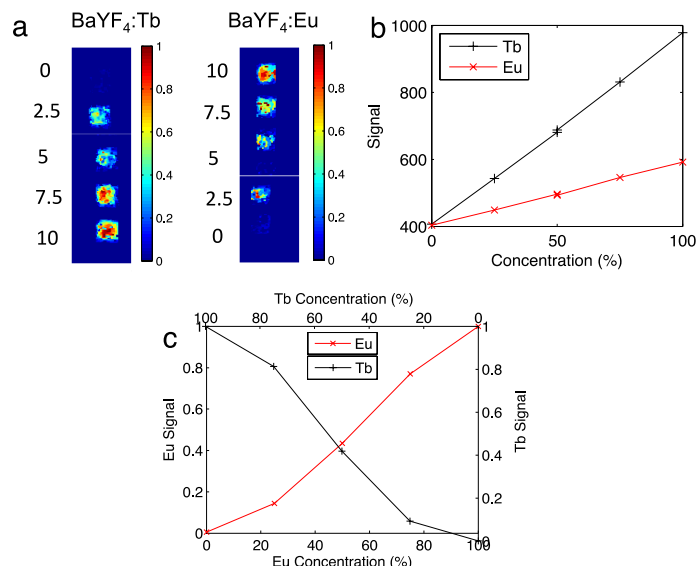


Figure 2: (a) Shown are the Ba_{0.55}Y_{0.3}F₂:Tb³⁺ and Ba_{0.55}Y_{0.3}F₂:Eu³⁺ phosphor concentrations with increasing/decreasing concentration (top-to-bottom) of Ba_{0.55}Y_{0.3}F₂:Tb³⁺ / Ba_{0.55}Y_{0.3}F₂:Eu³⁺, respectively. (b) The raw signal detected for each respective nanophosphor. (c) The relative median recovered concentration in each ROI plotted with respect to concentration.

To demonstrate this method in a pre-clinical mouse model, four batches of RLNPs were each mixed with 52 μ Ci (Curie) of activity of 18-F and Matrigel (BD Biosciences, Sparks, MD) and injected into both forelegs and flanks of a euthanized nude mouse, with Eu³⁺-doped RLNPs (Eu) only on the left foreleg, Tb³⁺-doped RLNPs (Tb) only on the left flank, an equal mixture of Eu³⁺-doped RLNPs and Tb³⁺-doped RLNPs (Mix) on the right flank, and an inactive undoped nanophosphor control (Ctrl) on the right foreleg. The locations of the subcutaneously injected RLNPs are shown in Figure 3(a). The feasibility of this method in a pre-clinical subject with X-ray excitation is shown in Figure 3(b)-(d). Tb³⁺-doped RLNPs embedded in the left and right flanks are shown successfully recovered in Figure 3(b). The Eu³⁺-doped RLNPs in the left foreleg and the right flank are shown successfully recovered in Figure 3(c). As a control, inactive RLNPs in the right foreleg did not luminesce. Figure 3(d) shows the results of the spectral unmixing algorithm, with the Eu³⁺-doped RLNPs shown in red, and the Tb³⁺-doped RLNP shown in green. The yellow in the multiplexed image indicates the presence of both types of nanophosphors.

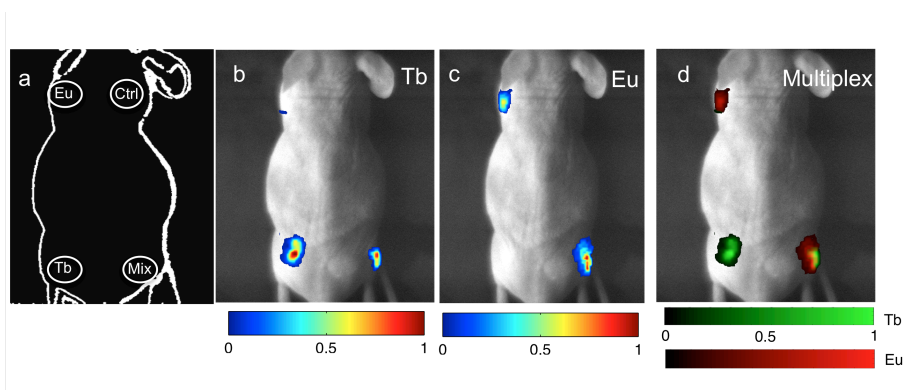


Figure 3: X-ray Luminescence: (a) Schematic of the locations of each type of RLNP. The inactive particles are indicated with the abbreviation (Ctrl). (b,c) The unmixed signal from the $Ba_{0.55}Y_{0.3}F_2:Tb$ and $Ba_{0.55}Y_{0.3}F_2:Eu$ particles, respectively. (d) The unmixed multiplexed image with colorbars for the relative concentrations of $Ba_{0.55}Y_{0.3}F_2:Tb$ and $Ba_{0.55}Y_{0.3}F_2:Eu$.

Research Accomplishments: SOW Aim 2: Imaging Hardware: Biopsy Needle – based RLI

Currently, biopsy is guided by X-ray fluoroscopy or ultrasound; these imaging modalities do not offer the ability to image molecular contrasts of tissue, and thus are limited in their ability to localize cancer. This shortcoming is especially true in small cancerous lesions, where structure visible by X-rays or ultrasound is not yet established; there is no current suitable means to localize cancers at this critical stage.

To meet this need, as outlined in Aim 2, a custom biopsy RLI catheter was fabricated to demonstrate proof-of-principle for phosphor image-guided biopsy procedures. The specifications were to provide a < 10 gauge imaging instrument that would fit down the needle bore. The ability to image is paramount to enable a visualization of the target mass, and to enable the search for the molecular beacon. The schematic of this instrument, shown in Figure 4, utilizes a water-cooled electron multiplied CCD (ProEM, Princeton Instruments) attached to the appropriate 4:1 magnification lenses (35mm and 8mm, Edmunds Optics, Megapixel) to project the proximal end of a leached fiber bundle (Schott, Inc.) onto the full CCD field of view. This fiber bundle is protected by a heat shrink catheter made of PTFE to prevent kinking and breaking of the individual fibers.

Images of the detection hardware and lens-coupled fiber are shown in Figure 5. The biopsy imaging system was tested for focus by imaging a business card under white-light illumination; an example image is shown in Figure 5c.

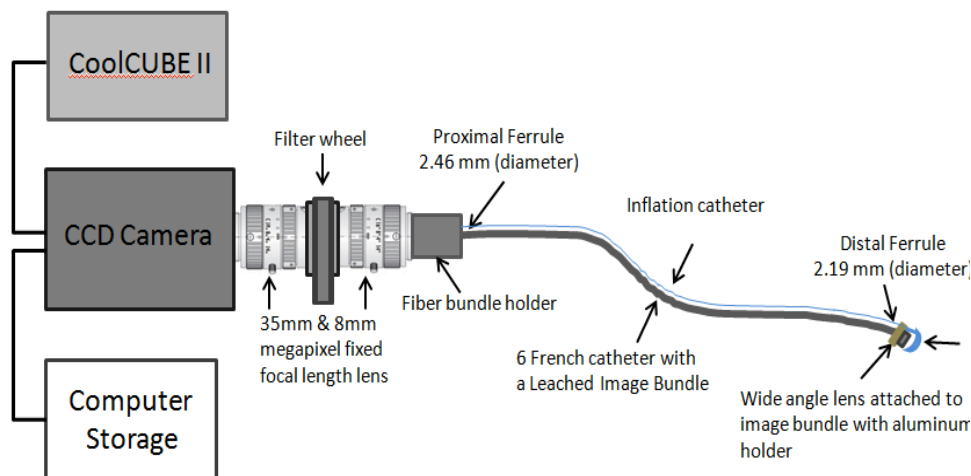


Figure 4: Schematic of the RLI biopsy device, consisting of a cooled CCD, a filter wheel for multiplexing ability, and a lens at the distal tip.

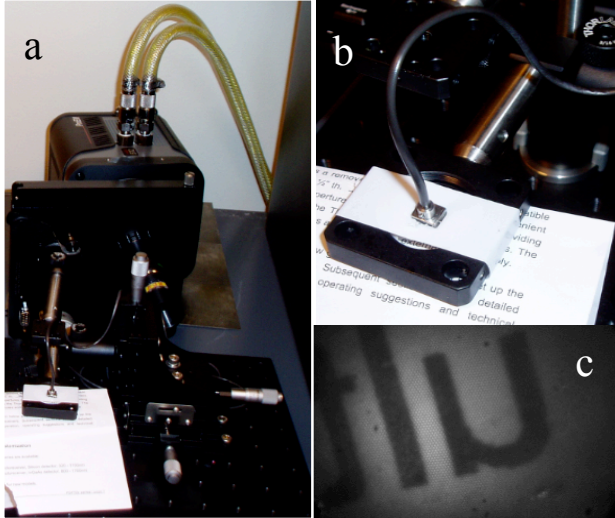


Figure 5: (a,b) Photographs of the Radioluminescent Biopsy Imaging device, specifically of (a) the CCD camera, filter wheel, and coupling optics; (b) a close-up of the distal tip of the catheter. (c) white-light image of text from a business card taken with the RLI biopsy device.

Training Accomplishments: SOW Aim 2: Imaging Hardware Development

In performing these tasks, the investigator gained valuable training in optical systems and catheter-based devices. This experience will be useful for future device development. In addition, the investigator gained valuable experience in working with small-animal phantoms (post-mortum) for more biologically appropriate phantom demonstration, where the tissue properties and geometries match that of the living subjects.

Research Accomplishments: SOW Aim 3: Imaging Hardware Development: Sensitivity Comparison

Towards meeting aim 3, we investigated the sensitivity of RLI and compared it to the current state-of-the-art in fluorescence molecular imaging. To capture sensitivity for the RLI system, we imaged decreasing concentrations of CaF₂:Eu, coated with Au, phosphor mixed with 1% agar. As shown in Figure 6a, we were able to linearly recover concentrations of phosphor to 10 μg/ml, or about 15nM. This compares favourably to fluorescence imaging, shown in Figure 6b [1], which has a sensitivity limitation of about 5nM.

However, RLI can be improved. As is apparent in Figure 6a, our investigations have uncovered a potential limit to sensitivity. While irradiating water-soluble phosphor samples, we discovered that X-rays create optical luminescence in water[2,3], which has been attributed to hydroxide radicals and hydrated electrons in the literature. This signal adds background signal to RLI, potentially limiting sensitivity to 20 μg/ml, or 30nM, as shown below.

After extensive investigations, we are in the process of developing a technique to minimize this effect. Specifically, this technique utilizes the fact that phosphors after-glow, while water does not. Afterglow results from long-lived phosphorescent states in the phosphor which temporarily traps electron-hole pairs before they combine with a luminescent center. This delay can be up to a few seconds in some phosphors, but does not exist in water. Thus, after-glow can be used to differentiate the phosphor signal from the water luminescence. We are currently experimentally testing this strategy for a further improvement in sensitivity.

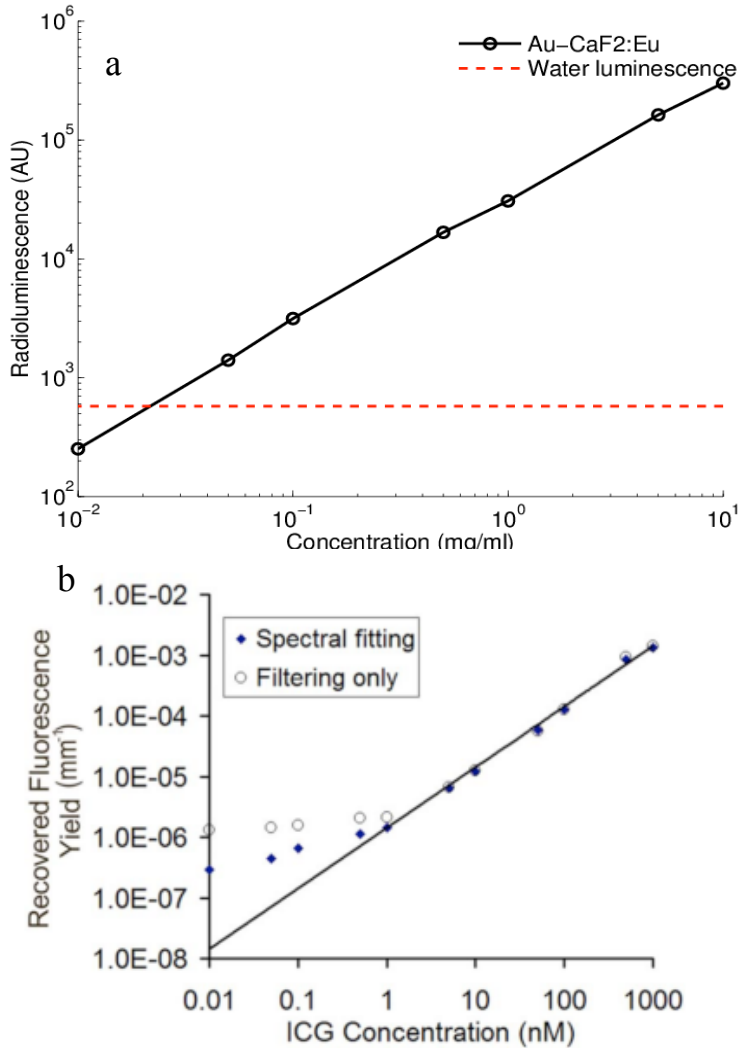


Figure 6: (a) Sensitivity of Radioluminescence imaging. The signal from several phantoms with concentrations ranging from 10 μ g/ml to 10 mg/ml is shown in black. The background water luminescence is shown in red. (b) Sensitivity of fluorescence imaging for two different filtering strategies (from [1]). The fluorescence sensitivity is limited by the autofluorescence in the tissue, or in this case, the autofluorescence of lipid in the intralipid / Indocyanine green phantom.

KEY RESEARCH ACCOMPLISHMENTS

- Improved instrumentation through leaded glass and emission filters to enable sensitivity of Radioluminescent Imaging to 30nM. This is sufficient for molecular imaging *in vivo* in small animals, per aim 4.
- Developed strategy to remove water-luminescent component to improve sensitivity.
- Demonstrated multiplexing ability of RLI in phantoms and small animal phantoms, and completed both hardware and software requirements.
- Fabricated an imaging fiber-based RLT biopsy system to demonstrate proof-of-concept.
- Engaged new mentor, Dr Fred Dirbas, Breast Surgeon and Intraoperative Radiation Therapy expert

REPORTABLE OUTCOMES:

1 journal publications, first author; 4 conference abstracts, and 2 conference presentations; Several postdoctoral fellows are now being mentored and working in RLI.

Oral Conference Presentations:

- **Carpenter, CM.**, et al.. “Towards ntraoperative Guidance for Breast Radiotherapy,” Presented at Novel Treatment Delivery Techniques, American Society for Therapeutic Radiology and Oncology, Miami, FL, Nov. 2011.
- **Carpenter, CM.** “Multiplexed Radioluminescence Tomography for Molecular Imaging,” Presented at the American Association of Medical Physics, Vancouver, CN.

Journal Publications:

- **Carpenter CM.**, et al. “Radioluminescent Nanophosphors Enable Multiplexed Small-Animal Imaging,” Opt Ex, 2012.

CONCLUSION

The second funding period has focused on the difficult task of optimizing the instrumentation to enable *in vivo* Radioluminescent Imaging. The incorporation of hardware and software innovations has resulted in nanoMolar sensitivity, which is sufficient for small animal imaging. In addition, the multiplexing imaging method is a vital solution to the research and development of molecular imaging, by enabling multiple molecular targets to be simultaneously imaged. This innovation will result in a reduction in research resources. A fully functioning fiber-based biopsy system has been developed, per aim 2. Sensitivity is now well-understood, per the goal of Aim 3, and thus research in live small animal models, the goal of aim 4, is now appropriate. In addition, this funding period has resulted in more molecular imaging training for the PI, and experience in mentoring other fellows.

The research and training completed, and yet-to-be completed in this grant are significant for the eradication of breast cancer, and for training for future novel tools for early detection of breast cancer. The coursework and experience gained by this PI will be critical in his goal to translate breast cancer treatment technology into the clinic.

REFERENCES

[1] Davis, SC, “Diffuse Tomography of Absorbing Fluorescent Optical Exogenous Contrast Guided by Simultaneously Acquired Magnetic Resonance Images,” Thesis, Dartmouth College Thayer School of Engineering, 2008.

[2] Quickenden, TI and Que Hee, SS. “The Luminescence of Water Excited by Ambient Ionizing Radiation,” Radiation Research, 46 (1) 1971.

[3] Tarasov, MD., El’yash, SL., Goncharova, VF., Petrushin, ON., Savel’ev, YA., Tarakanov, MY., Shigaev, YS. “Efficiency of Radioluminescence of Water under the Action of Accelerated Electrons,” Instruments and Experimental Techniques, 50(6), 1997.

APPENDIX

Radioluminescent nanophosphors enable multiplexed small-animal imaging

Colin M Carpenter,¹ Conroy Sun,¹ Guillem Pratx,¹ Hongguang Liu,² Zhen Cheng,² and Lei Xing^{1,*}

¹Department of Radiation Oncology, School of Medicine, Stanford University, Stanford, CA USA 94305 USA
²Molecular Imaging Program at Stanford (MIPS), Department of Radiology and Bio-X Program, Canary Center at Stanford for Cancer Early Detection, Stanford University, California, 94305-5344 USA
[*lei@stanford.edu](mailto:lei@stanford.edu)

Abstract: We demonstrate the ability to image multiple nanoparticle-based contrast agents simultaneously using a nanophosphor platform excited by either radiopharmaceutical or X-ray irradiation. These radioluminescent nanoparticles emit optical light at unique wavelengths depending on their lanthanide dopant, enabling multiplexed imaging. This study demonstrates the separation of two distinct nanophosphor contrast agents in gelatin phantoms with a recovered phosphor separation correlation of -0.98 . The ability to distinguish the two nanophosphors and a Cerenkov component is then demonstrated in a small animal phantom. Combined with the high-resolution potential of low-scattering X-ray excitation, this imaging technique may be a promising method to probe molecular processes in living organisms.

©2012 Optical Society of America

OCIS codes: (110.4234) Multispectral and hyperspectral imaging; (170.0170) Medical optics and biotechnology; (160.4236) Nanomaterials.

References and links

1. M. Stroh, J. P. Zimmer, D. G. Duda, T. S. Levchenko, K. S. Cohen, E. B. Brown, D. T. Scadden, V. P. Torchilin, M. G. Bawendi, D. Fukumura, and R. K. Jain, "Quantum dots spectrally distinguish multiple species within the tumor milieu in vivo," *Nat. Med.* **11**(6), 678–682 (2005).
2. X. Wu, H. Liu, J. Liu, K. N. Haley, J. A. Treadway, J. P. Larson, N. Ge, F. Peale, and M. P. Bruchez, "Immunofluorescent labeling of cancer marker Her2 and other cellular targets with semiconductor quantum dots," *Nat. Biotechnol.* **21**(1), 41–46 (2003).
3. W. Cai, D.-W. Shin, K. Chen, O. Gheysens, Q. Cao, S. X. Wang, S. S. Gambhir, and X. Chen, "Peptide-labeled near-infrared quantum dots for imaging tumor vasculature in living subjects," *Nano Lett.* **6**(4), 669–676 (2006).
4. F. G. Blankenberg, "In vivo detection of apoptosis," *J. Nucl. Med.* **49**(Suppl 2), 81S–95S (2008).
5. X. Gao, W. C. W. Chan, and S. Nie, "Quantum-dot nanocrystals for ultrasensitive biological labeling and multicolor optical encoding," *J. Biomed. Opt.* **7**(4), 532–537 (2002).
6. I. L. Medintz, H. T. Uyeda, E. R. Goldman, and H. Mattoussi, "Quantum dot bioconjugates for imaging, labelling and sensing," *Nat. Mater.* **4**(6), 435–446 (2005).
7. A. P. Alivisatos, W. Gu, and C. Larabell, "Quantum dots as cellular probes," *Annu. Rev. Biomed. Eng.* **7**(1), 55–76 (2005).
8. C. Sun, C. Carpenter, G. Pratx, and L. Xing, "Facile Synthesis of Amine-Functionalized Eu³⁺-Doped La(OH)₃ Nanophosphors for Bioimaging," *Nanoscale Res. Lett.* **6**(24), (2011).
9. H. Chander, "Development of nanophosphors - A review," *Mater. Sci. Eng. Rep.* **49**(5), 113–155 (2005).
10. J. Shen, L.-D. Sun, and C.-H. Yan, "Luminescent rare earth nanomaterials for bioprobe applications," *Dalton Trans.* **24**(42), 5687–5697 (2008).
11. C. M. Carpenter, C. Sun, G. Pratx, R. Rao, and L. Xing, "Hybrid x-ray/optical luminescence imaging: characterization of experimental conditions," *Med. Phys.* **37**(8), 4011–4018 (2010).
12. G. Pratx, C. M. Carpenter, C. Sun, and L. Xing, "X-ray luminescence computed tomography via selective excitation: a feasibility study," *IEEE Trans. Med. Imaging* **29**(12), 1992–1999 (2010).
13. C. Sun, G. Pratx, C. M. Carpenter, H. Liu, Z. Cheng, S. S. Gambhir, and L. Xing, "Synthesis and radioluminescence of PEGylated Eu(3+) -doped nanophosphors as bioimaging probes," *Adv. Mater. (Deerfield Beach Fla.)* **23**(24), H195–H199 (2011).
14. H. Liu, X. Zhang, B. Xing, P. Han, S. S. Gambhir, and Z. Cheng, "Radiation-luminescence-excited quantum dots for in vivo multiplexed optical imaging," *Small* **6**(10), 1087–1091 (2010).

15. R. S. Dothager, R. J. Goiffon, E. Jackson, S. Harpstrite, and D. Piwnica-Worms, "Cerenkov radiation energy transfer (CRET) imaging: a novel method for optical imaging of PET isotopes in biological systems," *PLoS ONE* **5**(10), e13300 (2010).
 16. M. A. Lewis, V. D. Kodibagkar, O. K. Öz, and R. P. Mason, "On the potential for molecular imaging with Cerenkov luminescence," *Opt. Lett.* **35**(23), 3889–3891 (2010).
 17. J. Axelsson, S. C. Davis, D. J. Gladstone, and B. W. Pogue, "Cerenkov emission induced by external beam radiation stimulates molecular fluorescence," *Med. Phys.* **38**(7), 4127–4132 (2011).
-

1. Introduction

The application of luminescent nanoparticles, such as quantum dots, in diagnostic molecular imaging is receiving much attention due to the potential to improve the differentiation between normal and malignant tissue by identifying signatures of disease [1]. For example, multicolored quantum dots enable the ability to probe multiple signatures of disease simultaneously; this is recognized to be potentially more beneficial than visualizing a single species [2]. Examples of these molecular markers include the $\alpha_v\beta_3$ integrin and VEGF receptors as indicators for vascular angiogenesis [3], and the translocation of phosphatidylserine for apoptosis [4]. The advantage of nanoparticles in this context is that they may be tuned to emit at varying wavelengths, without severely altering their physical structure [5]. Although quantum dots have been investigated extensively for biological applications [6, 7], nanophosphors have been relatively ignored. Like quantum dots, nanophosphors have high quantum efficiencies, sharp emission peaks, high photostability, and emission wavelength tunability [8, 9]. Nanophosphors have a distinct advantage in that they may emit light when irradiated by ionizing radiation, a process called radioluminescence. This work demonstrates the multiplexing potential of these nanophosphors, using an exemplary nanophosphor system.

While radioluminescence of phosphor material has long been used in radiation detectors, the use of radioluminescent nanophosphors (RLNPs) in biological contexts is just beginning to be explored [10]. Novel applications currently under investigation for radioluminescent imaging (RLI) include direct biological feedback of molecular changes and tumor burden during radiation treatment. This information may be used as a means to enhance radiation treatment efficacy. In addition, RLI may be used to probe molecular information at a superior resolution to other molecular imaging modalities, such as Fluorescence Molecular Tomography (FMT), Positron Emission Tomography (PET), and Single Photon Computed Emission Tomography (SPECT), by collimating the excitation X-ray beam. This high-resolution technique, called X-ray Luminescence (Computed) Tomography (XLCT), utilizes narrowly-collimated X-ray beams to resolve deep-seated RLNPs. This is made possible because of the very low X-ray scatter in small-animals [11, 12].

This study demonstrates the potential use of RLNPs doped with different rare-earth luminescent centers to enable multiplexed RLI after excitation by ionizing radiation. In particular, it demonstrates the ability to recover the concentrations of each RLNP from multispectral images of the subject. To highlight the flexibility of this technique, multiplexed imaging was demonstrated using two different excitation schemes: radiopharmaceuticals (^{18}F) and X-ray radiation.

2. Methods

2.1 Imaging hardware

A custom imaging system was built to image and measure the concentrations of the nanophosphor contrast agents. A 512x512 pixel back-illuminated deep-cooled (-70C) CCD camera (ProEM, Princeton Instruments, Trenton, NJ) was outfitted with a F/#0.95 imaging lens (DO-5095, Navitar, Rochester, NY), and leaded glass was placed above the subject. Optical bandpass filters (546nm \pm 10nm for Tb^{3+} doped RLNPs, 700nm \pm 20nm for Eu^{3+} doped RLNPs; Andover Corporation, Salem, NH) were placed in front of the camera lens to

selectively collect emitted light in the unique spectral regions. A motorized platform adjusted the working distance of the camera to the subject and controlled the field of view. This imaging box was placed in the path of a superficial X-ray unit (Pantax Therapax, East Haven, CT), with voltage and current set to the X-ray tube 90keV and 10mA. This system was operated remotely from the control room of the X-ray unit, outside the X-ray room [11].

Optical spectra from the RLNPs (Fig. 1(a) and Fig. 1(b)) was collected by measuring the emission of dry powder samples in cuvettes. The distal end of a 10m 400 μ m optical fiber was placed in contact with the side of cuvettes containing each sample, while the proximal end was attached to a spectrophotometer (SP2150, Princeton Instruments) connected to the CCD camera, which was operated from the X-ray control room. Optical emission spectra within the visible and NIR range was acquired with custom software written in Labview (National Instruments, Austin, TX). By acquiring vertical spectral bins for each wavelength, image processing was used to remove X-ray noise, which stochastically appeared in the CCD. Alternatively, Cerenkov spectra was recorded by fitting a quadratic curve to data collected from a commercial imaging system (IVIS Spectrum, Perkin Elmer, Waltham, MA). The signal emitted from the radiopharmaceuticals was verified via a small animal Positron Emission Tomography (PET) system (Siemens R4 Micro-PET, Malvern, PA).

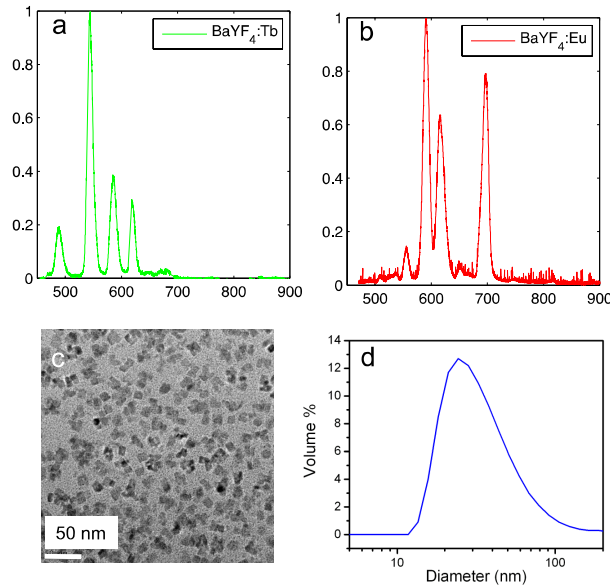


Fig. 1. (a) Radioluminescent spectrum of the $\text{Ba}_{0.55}\text{Y}_{0.3}\text{F}_2:\text{Tb}^{3+}$ particles, which emit primarily in the green. (b) Radioluminescent spectrum of the $\text{Ba}_{0.55}\text{Y}_{0.3}\text{F}_2:\text{Eu}^{3+}$ particles, which emit primarily in the red and near-infrared. (c) Transmission electron microscopy image of the RLNPs. (d) Hydrodynamic size distribution of the RLNPs as determined by dynamic light scattering.

2.2 Contrast agent synthesis

In this study, we demonstrate two possible dopants, europium (Eu^{3+}) and terbium (Tb^{3+}). A detailed description of the synthesis of these particles was recently described by Sun et al. [13]. The host barium yttrium fluoride ($\text{Ba}_{0.55}\text{Y}_{0.3}\text{F}_2$) nanocrystals were doped with either terbium (0.5%) or europium (0.5%) to produce emission maxima at 541nm and 586nm, respectively. Both RLNPs emitted additional spectral peaks towards the near infrared (NIR) at 629nm and 692nm, respectively, as seen from Fig. 1(a) and Fig. 1(b); these emission wavelengths enable imaging of deeper structures. The unique signatures emitted by each phosphor enabled the ability to perform multiplexing. The surfaces of the RLNPs were

modified with poly(ethylene glycol) (PEG, MW 600) through a ligand exchange process to achieve colloidal stability in aqueous solutions. These phosphors can be functionalized with a biotin linker bound to the PEG. Shown in Fig. 1(c) is the transmission electron microscopy (TEM) image of this RLNP platform with a cubic morphology and mean particle size of 14nm. The hydrodynamic size was determined by dynamic light scattering (DLS); particles with hydrodynamic size of ~ 27 nm were the most common, as shown in Fig. 1(d).

2.3 Image multiplexing

To form images of the concentrations, c , of each of these particles, the light emitted, ϕ , was recorded over the several optical spectral regions defined by filter f_1 and filter f_2 to form images of the subject, $i_1 = \phi(f_1)$ and $i_2 = \phi(f_2)$. These images, and the pre-recorded reference spectra, ϵ , for $\text{Ba}_{0.55}\text{Y}_{0.3}\text{F}_2:\text{Tb}^{3+}$, (ϵ_{Tb}), $\text{Ba}_{0.55}\text{Y}_{0.3}\text{F}_2:\text{Eu}^{3+}$, (ϵ_{Eu}), and the Cerenkov luminescence, (ϵ_{Ch}), were input into a linear-least squares algorithm to extract the contributions from each nanophosphor. Reference spectra was collected with a calibrated spectrometer, thus enabling a quantitative comparison between the nanophosphors. Since Cerenkov light was generated from the F-18 radiotracer, it was necessary to account for the Cerenkov component for the experiments involving radiotracer excitation. For experiments involving X-ray excitation, the Cerenkov component was not present, since Cerenkov light arises from photons emitted from highly-energetic charged particles that are greater than the energy of charged particles created during X-ray excitation.

2.4 Experimental demonstration

To validate the ability of this method to image multiple nanophosphors simultaneously, five phantoms (99% DI water, 1% agarose) were fabricated containing Tb^{3+} and Eu^{3+} doped RLNPs of linearly varying concentrations (in units of mg/ml) and mixed in the following ratios: (0:10; 2.5:7.5; 5:5; 7.5:2.5; and 10:0). To demonstrate this method in a pre-clinical mouse model, four batches of RLNPs were each mixed with 52 μCi (Curie) of activity of 18-F and Matrigel (BD Biosciences, Sparks, MD) and injected into both forelegs and flanks of a nude mouse, with Eu^{3+} -doped RLNPs (Eu) only on the left foreleg, Tb^{3+} -doped RLNPs (Tb) only on the left flank, an equal mixture of Eu^{3+} -doped RLNPs and Tb^{3+} -doped RLNPs (Mix) on the right flank, and an inactive undoped nanophosphor control (Ctrl) on the right foreleg. For the radioisotope-excited experiment, the subject was imaged immediately after injection. For the X-ray-excited experiment several days later (after the 18-F had fully decayed), the same subject was placed in the imaging apparatus and excited by a 90keV X-ray source, which was transmitted through the dark-box. The same subject was imaged with the X-ray and radiopharmaceutical excitation on separate days to allow the radioisotope to decay thoroughly. Concentration images of the animals were normalized due to the lack of recorded tissue optical properties.

3. Results

3.1 Phantom validation

Fig. 2(a) displays the unmixed images for linearly increasing (top-to-bottom) amounts of Tb^{3+} -doped RLNPs on the left, and decreasing (top-to-bottom) Eu^{3+} -doped RLNPs on the right, at each concentration. The median values for each region of interest were plotted with respect to concentration. Fig. 2(b) shows the median raw signal detected from each nanophosphor concentration. Fig. 2(c) demonstrates this method's efficacy in separating the nanophosphors; the correlation between the samples was ($r = -0.98$).

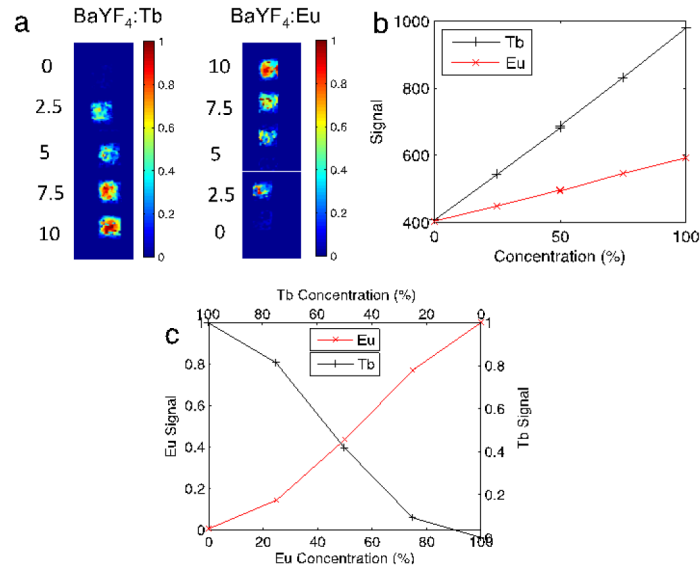


Fig. 2. (a) Shown are the $\text{Ba}_{0.55}\text{Y}_{0.3}\text{F}_2:\text{Tb}^{3+}$ and $\text{Ba}_{0.55}\text{Y}_{0.3}\text{F}_2:\text{Eu}^{3+}$ phosphor concentrations with increasing/decreasing concentration (top-to-bottom) of $\text{Ba}_{0.55}\text{Y}_{0.3}\text{F}_2:\text{Tb}^{3+}$ / $\text{Ba}_{0.55}\text{Y}_{0.3}\text{F}_2:\text{Eu}^{3+}$, respectively. (b) The raw signal detected for each respective nanophosphor. (c) The relative median recovered concentration in each ROI plotted with respect to concentration.

3.2 Animal phantom validation

The locations of the subcutaneously injected RLNPs are shown in Fig. 3(a). The feasibility of this method in a pre-clinical subject with X-ray excitation is shown in Figs. 3(b)-3(d). Tb^{3+} -doped RLNPs embedded in the left and right flanks are shown successfully recovered in Fig. 3(b). The Eu^{3+} -doped RLNPs in the left foreleg and the right flank are shown successfully recovered in Fig. 3(c). As a control, inactive RLNPs in the right foreleg did not luminesce. Fig. 3(d) shows the results of the spectral unmixing algorithm, with the Eu^{3+} -doped RLNPs shown in red, and the Tb^{3+} -doped RLNP shown in green. The yellow in the multiplexed image indicates the presence of both types of nanophosphors.

The results of RLI with radiopharmaceutical excitation are shown in Fig. 4 (performed several days prior but on the same mouse as Fig. 3). The PET image of the four injected regions of ^{18}F with active and inactive particles is shown in Fig. 4(a); this image is included for spatial validation. All corners illuminate in the PET image because of the injection of ^{18}F with all particles. The unmixed Cerenkov image is shown in Fig. 4(b). Note the Cerenkov signal in each region, due to the injection of ^{18}F in each region; these correspond to the regions in the PET image. In particular, note the recovery of the Cerenkov light in the right foreleg, which contained the inactive control $\text{Ba}_{0.55}\text{Y}_{0.3}\text{F}_2$ nanocrystals along with ^{18}F . The successful recovery of Tb^{3+} -doped RLNPs and Eu^{3+} -doped RLNPs is demonstrated in Figs. 4(c)-4(d). The spectrally unmixed fused image is shown in Fig. 4(e), with Eu^{3+} -doped RLNPs in red, Tb^{3+} -doped RLNPs in green, and Cerenkov light in blue. Note that the doped nanoparticles did not emit in the control foreleg.

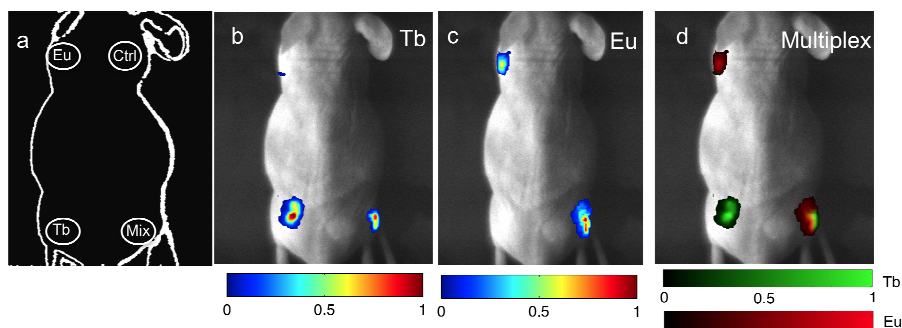


Fig. 3. X-ray Luminescence: (a) Schematic of the locations of each type of RLNP. The inactive particles are indicated with the abbreviation (Ctrl). (b,c) The unmixed signal from the $\text{Ba}_{0.55}\text{Y}_{0.3}\text{F}_2\text{:Tb}$ and $\text{Ba}_{0.55}\text{Y}_{0.3}\text{F}_2\text{:Eu}$ particles, respectively. (d) The unmixed multiplexed image with colorbars for the relative concentrations of $\text{Ba}_{0.55}\text{Y}_{0.3}\text{F}_2\text{:Tb}$ and $\text{Ba}_{0.55}\text{Y}_{0.3}\text{F}_2\text{:Eu}$.

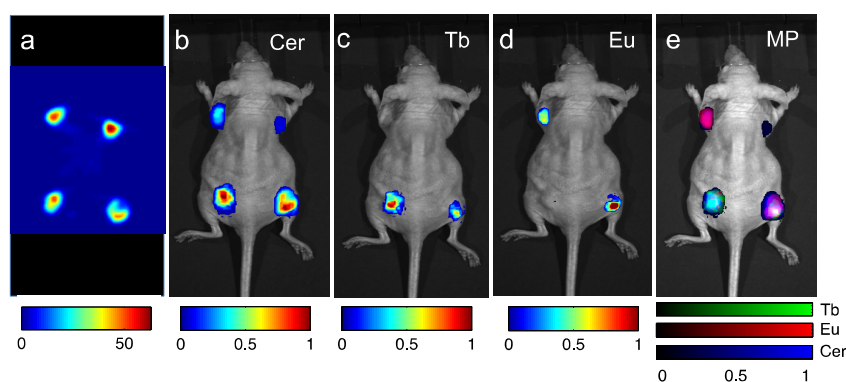


Fig. 4. Radiopharmaceutical luminescence: (a) Positron emission tomography image of the relevant RLNPs. (b) The unmixed signal from Cerenkov emission. (c,d) Unmixed signal from the $\text{Ba}_{0.55}\text{Y}_{0.3}\text{F}_2\text{:Tb}^{3+}$ particles and $\text{Ba}_{0.55}\text{Y}_{0.3}\text{F}_2\text{:Eu}^{3+}$ particles, respectively. (e) Unmixed multiplexed image with colorbars for the relative contributions of $\text{Ba}_{0.55}\text{Y}_{0.3}\text{F}_2\text{:Tb}^{3+}$, $\text{Ba}_{0.55}\text{Y}_{0.3}\text{F}_2\text{:Eu}^{3+}$, and Cerenkov emission.

4. Discussion and conclusions

The methods outlined in this paper demonstrate the ability of this particle system to simultaneously be used for multiple types of RLI; these may then be attached to distinct molecular targets. RLNPs may become an important analog to the current tools dedicated to pre-clinical imaging due to their great versatility. In one application, if injected with a radiopharmaceutical, the nanoparticles introduced in this study would enable multiple-targeting; this could prove to be an important method to identify the kinetics or accumulation after drug-injection. These RLNPs may also aid in the down-conversion of Cerenkov light emitted from the radiopharmaceutical [14–17]. In another application, these RLNPs may be used in conjunction with X-ray luminescence computed tomography [12] to recover high-resolution molecular-specific images. In yet another application, this RLNP system may aid in the on-line identification of response to radiation therapy. Through targeting of molecular markers specific for tumors, this method could provide feedback during therapy as to the status of treatment; the penetration of high-energy photons in conjunction with a light detector would ensure the ability to reach a larger depth in tissue.

In conclusion, we have demonstrated a nanoparticle platform for radioluminescence imaging which may be used to image multiple nanophosphors simultaneously using both radiopharmaceutical and X-ray irradiation. We showed an inverse relationship between

concentrations of the types of RLNPs, which showed successful separation of the contribution from the two emission signals. We then demonstrated this technology in a small-animal model.

Acknowledgments

The authors gratefully acknowledge the Department of Defense Breast Cancer Research Programs W81XWH-10-1-0506 (CMC), W81XWH-11-1-0087 (CS), and W81XWH-11-1-0070 (GP), the National Institutes of Health ICMIC P50CA114747, and the Center for Biomedical Imaging at Stanford-CBIS (CMC) for funding.